Bulletin of the
Seismological Society of America

Vol. 70 August 1980 No. 4

LONG-PERIOD GROUND MOTION FROM A GREAT EARTHQUAKE

By Rhett Butler* and Hiroo Kanamori

ABSTRACT

Direct body waves and fundamental surface waves are calculated for a credible, hypothetical great earthquake on the San Andreas Fault. The prototype event assumed is the Fort Tejon earthquake of January 9, 1857. Amplitudes and durations of long-period ground motion ($T > 1$ sec) are found for a receiver in downtown Los Angeles. Calculations are carried out for various epicenters, dislocation profiles, and time functions. Ground motion from Love radiation is found to be most important, with peak-to-peak amplitudes up to 14 cm and durations up to 5 min. This duration is a factor of 3 longer than has been assumed by previous design earthquakes whose estimates have been based upon acceleration criteria. Although the present result reveals several important features of long-period ground motion resulting from a great earthquake, more details of rupture propagation need to be known before a more definitive prediction can be made. The present result should be considered tentative.

Introduction

Shaking or strong ground motion due to the release of elastic energy from the faulting process is the primary cause of damage from most earthquakes. Thus, the study of strong ground motion has naturally been the concern of many seismologists and earthquake engineers. Stricter building codes in areas of appreciable earthquake hazard, and building designs more resistant to earthquake shaking have been consequences of this research. The data on which most of these studies are based are strong motion accelerograms recorded in the epicentral area of earthquakes. However, only three records exist for magnitude 7 events, and no magnitude 8 events have been recorded (Jennings *et al.*, 1968). To circumvent this lack of data, various scaling arguments have been made to infer the nature of ground motion for a great earthquake from an understanding of smaller events (Jennings *et al.*, 1968; Hanks, 1976). These arguments may be qualitatively useful in the absence of empirical data, but leave much to be desired in terms of credible quantitative estimates from ground shaking from a great earthquake.

This paper will approach the problem of ground motions from a large earthquake from a direct modeling procedure. In recent years, seismologists have seen a large measure of success in modeling earthquake sources by simple dislocations in an elastic medium. Herrmann and Nuttli (1975a, b) applied dislocation theory to understand multiple-mode surface wave contributions to ground motions for moderate-sized earthquakes for a continental path. The applicability of simple dislocation theory methods for modeling ground motion as a function of the earthquake size and the period range of ground shaking will be considered. Justifying this

* Present address: 446 E. Poppyfields, Altadena, California 91001.

technique, the long-period ground motions are modeled from a hypothetical earthquake on the San Andreas Fault patterned after the Fort Tejon earthquake of January 9, 1857. These long-period ground motions ($T > 1$ sec) have little effect on ordinary structures. However, high-rise buildings, oil tanks, suspension bridges, reservoirs, and offshore oil-drilling platforms have natural resonances which lie in the long-period ranges.

The basic procedure is as follows. The segment of the San Andreas Fault system which broke during the 1857 event is subdivided into many small subsegments. The ground motion response of each subsegment is computed for direct body waves and fundamental surface waves for a receiver located in downtown Los Angeles. The responses of the subsegments are time-lagged and summed to simulate rupture propagation for several different epicenters. Smooth and nonsmooth rupture processes are considered. Uncertainties in the complexity of the rupture, velocity structure, and the effects of lateral heterogeneities preclude definitive results. However, tentative conclusions of the nature of long-period ground motion from a great earthquake may be reached for such gross parameters as overall amplitudes and durations.

The Model

In principle, if the geometric shape and size of the fault plane, S, the slip $\vec{D}(\vec{r}, t)$ on the fault plane as a function of position, $\vec{r}$, and time, t, and the structure of the propagation medium are known, one can accurately compute the ground motion. However, in actual problems, the slip $\vec{D}(\vec{r}, t)$ can be a very complex function, and the structure is not known in detail. Even if the structure is reasonably well known, it is usually laterally heterogeneous, and the computation of the response is exceedingly difficult. Various seismological studies during the past decade have, however, shown that under certain circumstances the ground displacement caused by an earthquake can be simulated by a simple model. At periods $T \geqq 1$ sec, it has been shown that for many small-to-moderate-size earthquakes (source dimension $L \leqq 30$ km), a relatively smooth simple dislocation model, and a very simple structure can explain both near-field ground motion and teleseismic data very well. Near-field studies include: 1966 Parkfield earthquake (Aki, 1968; Haskell, 1969), 1943 Tottori earthquake (Kanamori, 1972), 1971 San Fernando earthquake (Mikumo, 1973b; Trifunac, 1974), 1969 Gifu earthquake (Mikumo, 1973a), 1968 Saitama earthquake (Abe, 1974), 1968 Borrego Mountain earthquake (Heaton and Helmberger, 1977), 1973 Morgan Hill earthquake (Helmberger and Malone, 1975), and the 1976 Brawley earthquake (Heaton and Helmberger, 1978). Teleseismic studies include: 1967 Koyna earthquake (Langston, 1976), 1975 Oroville earthquake (Langston and Butler, 1977), 1968 Borrego Mountain earthquake (Burdick and Mellman, 1976), 1966 El Golfo earthquake (Ebel *et al.*, 1978), and the 1971 San Fernando earthquake (Langston, 1978).

As a specific example, the Helmberger and Malone (1975) study of the Morgan Hill earthquake modeled observed seismograms in the distance range 10 to 100 km by the generalized ray technique using a simple source time function and a layered structure. The close agreement between their synthetic seismograms and the observed suggests that a simple source embedded in a credible crustal model may explain many of the complexities in local field seismograms. However, even for these well-studied earthquakes listed above, very short-period ($T < 1$ sec) waves are difficult to explain.

When the source dimension becomes very large ($L \geqq 150$ km), the source process

cannot be modeled by a simple smooth dislocation source even for the period range $T \geqq 1$ sec. It is known that most large earthquakes are complex multiple shocks, e.g., the 1976 Guatemalan earthquake (Kanamori and Stewart, 1978). However, at very long periods ($T > 100$ sec), even such a large complex event can be modeled by a simple propagating dislocation source. Observed waveforms of long-period Rayleigh and Love waves can usually be explained very well by using a smooth propagating dislocation source and a laterally homogeneous gross earth model; e.g., Kanamori (1970), Kanamori and Cipar (1974), Kanamori and Stewart (1978), Stewart and Cohn (1978), Stewart (1978), and Butler *et al.* (1979).

The situation described above may be summarized schematically by Figure 1. The applicability and limitations of using a relatively smooth source in modeling a given earthquake is a function of the source dimension of the event and the period range of interest. The dividing line is only qualitative.

Considering now a large earthquake on the San Andreas Fault with a source dimension of 100 km or greater, it is clear from Figure 1 that for periods shorter

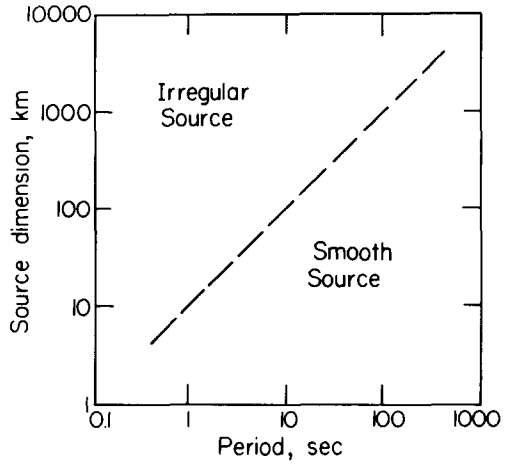

FIG. 1. The approximate applicability of a relatively smooth source is shown as a function of source dimension and period range of interest.

than 1 sec, a very complex source must be used. As a good model is not available for such a complex source, it would be difficult to make a meaningful numerical model of the ground shaking. In the period range 1 to 10 sec, the proximity of the dividing line is such that a more or less smooth source may be used to model the ground motion if some complexity is added. These periods, although not the high-frequency strong ground motion experienced in earthquakes, are nevertheless of engineering significance to large structures which have natural periods within this range.

The Fort Tejon earthquake of January 9, 1857 may be considered a prototype of a future great earthquake on the San Andreas Fault. This remarkable event, felt from Sacramento to Yuma, is associated with the most recent slippage along the Carrizo Plain and "big bend" sections of the San Andreas Fault System. Compilations by Wood (1955) and Agnew and Sieh (1978) of contemporary accounts, suggest that the earthquake was characterized by short-period strong ground motion in the meizo-seismal area, and longer period effects were felt over a much larger region. Seiching of rivers and lakes were reported as far north as Sacramento. Fissures in the earth, presumably due to liquefaction in soft ground, were reported near Ventura, North Long Beach, Fountain Valley, and San Bernardino. Faulting on the San

Andreas was observed along the segment from Lake Elizabeth to at least Cholame Valley. Although faulting accounts are consistent with right-lateral strike-slip motion, no contemporary accounts indicate the amount of offset.

Additional constraints on the faulting associated with the Fort Tejon earthquake may be inferred from recent geomorphological studies along the San Andreas. Wallace (1968) measured stream offsets in the Carrizo Plain. The data are scattered, but a clustering of values of 10 m (meters) is indicated. In a detailed geomorphic study of the San Andreas from Parkfield to San Bernardino, Sieh (1978) concurs with Wallace's 10 m in the Carrizo Plain, but reports evidence that the displacement may have been only one-half of that southeast of Tejon Pass. Trenching across the San Andreas at Pallette Creek (Sieh, 1978) indicates that fault movements associated

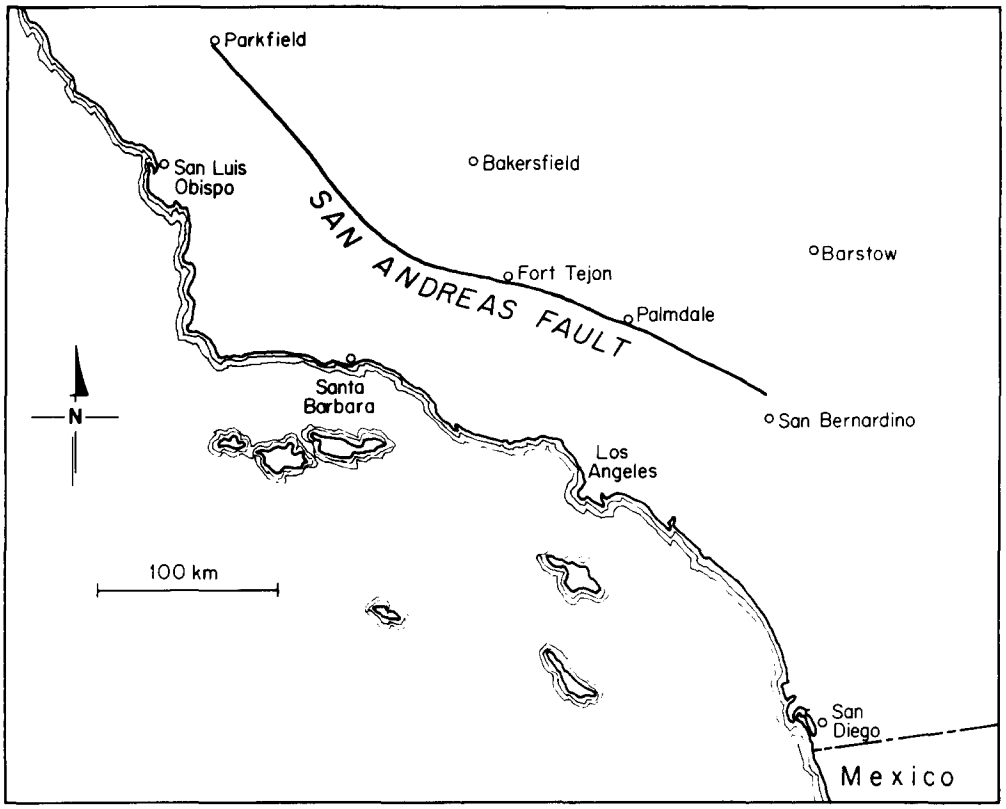

FIG. 2. The segment of the San Andreas Fault used in the modeling.

with the Fort Tejon earthquake extended at least to this location. There is some question as to the southern terminus of the faulting, but the absence of high intensities at San Bernardino would suggest that the rupture ceased north of this city. Trees tilted at Wrightwood indicate slippage to that point.

The limits and the geometry of the assumed Fort Tejon fault model are shown in Figure 2: a right-lateral, pure strike-slip fault extending 375 km from Parkfield to near San Bernardino. The depth of faulting is assumed to be 15 km over the length of the fault. This value is consistent with the maximum depth of earthquakes in southern California and is presumably a depth where fault creep or some other process substitutes for brittle fracture. This depth is also consistent with models for geodetic data from the 1906 San Francisco earthquake on the northern segment of the San Andreas. From the geomorphological work (Wallace, 1968; Sieh, 1978) on

stream offsets in the Carrizo Plain, a potential displacement of 10 m is considered credible. Given these assumptions the seismic moment, M_0, defined as

$$M_0 = \mu DS \tag{1}$$

(μ, rigidity; D, displacement; S, fault area) for the hypothetical event would be about 1.5×10^{28} dyne-cm.

For a laterally heterogeneous crustal structure, a meaningful numerical calculation of ground motion would be difficult, if not impossible. Seismic refraction surveys in southern California (Kanamori and Hadley, 1975) indicate that the region has a remarkably homogeneous crust. The crustal model obtained by Kanamori and Hadley (1975) is used with excellent success in locating local earthquakes in southern California by SCARLET (Southern California Array for Research on Local Earthquakes and Teleseisms). This study adopts a seismic model designated KHC2, incorporating the Kanamori and Hadley crustal model slightly modified to include a 1-km layer of sediment (see Table 1). Shear velocities are assumed from Poisson's ratio. For the purpose of calculating surface-wave excitation functions, this crustal model overlies a gross earth mantle, model C2 of Anderson and Hart (1976).

TABLE 1

KHC2 CRUST (ADAPTED FROM KANAMORI AND HADLEY, 1975)

Compressional Velocity (km/sec)	Shear Velocity (km/sec)	Density (ρ/cm^3)	Thickness (km)
2.5	1.4	2.5	1.0
5.5	3.1	2.6	3.0
6.3	3.6	2.7	23.4
6.8	3.9	2.9	5.0

Several important parameters—the epicenter, fault rupture velocity, and the dislocation particle velocity—must be assumed. The epicenter of the 1857 Fort Tejon earthquake is unknown. This study will consider three extreme cases: (1) an epicenter at Parkfield with rupture propagating toward Los Angeles; (2) an epicenter at the San Bernardino with the rupture propagating northward; (3) an epicenter at the point on the fault closest to Los Angeles, near Palmdale, and rupturing in a bilateral fashion. An average velocity of 2.5 km/sec and an average dislocation particle velocity of 1 m/sec are chosen in the present study. These values are consistent with determinations for other crustal earthquakes (e.g., Geller, 1976).

Figure 1 suggests that some degree of complexity must be included in the Fort Tejon source model. The manner in which the complexity is included is somewhat *ad hoc*, but has a basis within a conceptualization of the earthquake source. For earthquakes of small source dimension, they may be characterized by a rather simple smooth source model for periods $T \geqq 1$ sec. In modeling these small events with a dislocation source, it is sufficient to use only a single set of parameters—displacement, particle velocity, and rupture velocity—for the entire fault surface. For earthquakes of large source dimension, this treatment is inadequate. Two large strike-slip earthquakes, the 1967 Caracas earthquake (Rial, 1978) and the 1976 Guatemalan earthquake (Kanamori and Stewart, 1978), were found to be multiple shocks; a propagating sequence of smaller quasi-independent events filling the fault surface. Kanamori and Stewart (1978) envisaged these complex multiple shocks in

terms of a heterogeneous distribution of stress along the fault plane. This heterogeneity may be caused by asperities, differences in strength, differences in pore pressure, differences in slip characteristics (stable sliding versus stick-slip), or combinations of these factors.

In concordance with these concepts, complexity is added to the Fort Tejon source model in the following manner. The assumed dislocation parameters (displacement $D = 10$ m, particle velocity $\dot{D} = 1$ m/sec, and rupture velocity $V_R = 2.5$ km/sec) are viewed as average values for the fault. Piecewise along the fault, the parameters D, $\dot{D}$, and V_R vary about these average values. Over a local section of the fault, some coherence is expected in the parameters. Following Haskell (1966) and Aki (1967), a correlation length, k_L^{-1}, is introduced. Consider the displacement $D(x)$ to be

$$D(x) = D_0 + d(x) \tag{2}$$

where D_0 is the average offset over the fault, and $d(x)$ is the random variation about this average. Assuming that the autocorrelation of $d(x)$

$$A(\xi) = \int_{-\infty}^{\infty} d(x)\, d(x + \xi)\, dx \tag{3}$$

has the functional form

$$A(\xi) \sim e^{-k}L^{|\xi|}, \tag{4}$$

then the variation $d(x)$ will maintain a coherence over a length k_L^{-1}.

The amplitude spectrum of $d(x)$, $|\hat{d}(k)|$, is related to $A(\xi)$ by

$$|\hat{d}(k)|^2 = \int_{-\infty}^{\infty} A(\xi) e^{-ik\xi}\, d\xi. \tag{5}$$

Integrating, we have

$$|\hat{d}(k)| \sim \left(\frac{k_L}{k_L^2 + k^2}\right)^{1/2} \tag{6}$$

Now, choosing a phase spectrum, $\hat{d}$(k) can be retransformed to obtain $d(x)$ with the desired coherence property.

In practice for a fault, discretized into 2.5-km segments, $\hat{d}(k)$ is given by

$$\hat{d}(k_n) = \left(\frac{k_L}{k_L^2 + k_n^2}\right)^{1/2} e^{i\Psi_n} \tag{7}$$

where Ψ_n is a randomly generated phase and k_n the wavenumber. The variation $d(x)$ is then recovered by a Fast Fourier transform and the amplitude rescaled to the desired range of variation. The same treatment is followed for the particle velocity, $\dot{D}$, and rupture velocity, V_R.

In the computation of Fort Tejon body-wave radiation, we assumed two basic models. The first model simulates smooth rupture and thus, D, $\dot{D}$, and V_R are held

constant over the fault. Secondly, several random models were run with the displacement, D, ranging from 0 to 20 m with a correlation length of 10 km. The rise time ($\tau = D/\dot{D}$) and rupture velocity were held constant at, respectively, 10 sec and 2.5 km/sec.

The surface wave computations included a smooth model with D, $\dot{D}$, and V_R held constant and three different random models (see Table 2). The short correlation length of random model 2 produces the effect of an uncorrelated or totally random variation. Autocorrelations of the randomly varying models were recalculated to ensure agreement with the input correlation length.

All calculations in this paper are for the fault geometry assumed in Figure 2 and a receiver at downtown Los Angeles.

Body Waves

The De Hoop-Haskell method (De Hoop, 1958; Haskell, 1969) was used in computing the near-field, body-wave displacements. The fault assumed in Figure 2 was subdivided into one hundred and fifty 2.5-km segments. The expressions (3.1) to (4.3) in Haskell (1969) were numerically double-integrated over each fault segment placed in an infinite homogeneous medium with a P-wave velocity of 6.3 km/sec and S-wave velocity of 3.6 km/sec. The effect of the free surface was accounted for by doubling the amplitude in the whole space calculation.

TABLE 2

Surface-Wave Fault Models

Model Type	Correlation Length (km)	Displacement (m)	Particle Velocity (m/sec)	Rupture Velocity (km/sec)
Smooth	—	10.0	1.0	2.5
Random 1	10.0	10.0 ± 2.5	1.0 ± 0.5	2.5 ± 0.5
Random 2	0.1	10.0 ± 2.5	1.0 ± 0.5	2.5 ± 0.5
Random 3	10.0	10.0 ± 2.5	1.0 ± 1.0	2.5 ± 0.5

As mentioned earlier, for these body-wave calculations, the rise time of the slip dislocation for each fault segment was 10 sec, and a velocity of rupture of 2.5 km/sec was assumed. Thus, upon calculation of the displacement time history in Los Angeles from each fault segment, the displacements were summed from each of the segments shifting the time to account for the propagation of the rupture from the chosen epicenter.

Several of the models computed are shown in Figure 3. A quantitative measurement of the amplitudes and duration of ground motion for these synthetics in several period windows will be provided in the discussion section. It is useful at this time, however, to qualitatively describe these results. The *upper* part of Figure 3 shows horizontal body waves computed for a smooth and a random model with an epicenter at Parkfield, the rupture propagating toward Los Angeles. The *lower* part of the figure plots body waves from an epicenter at the San Bernardino end of the fault. The gross features exhibited by the smooth and random models are quite similar. The ground motions calculated for these two extreme epicenters are quite different. These differences are largely the result of two processes: the direction of rupture propagation and the change in the source radiation felt at Los Angeles as the geometry between fault and receiver change during the rupture propagation. The section of the fault from Parkfield to the Carrizo Plain contributes to only a minor part of the near-field displacements, as Los Angeles is nearly on the strike of the

fault. Thus, the motion from a Parkfield epicenter builds to the static value more slowly than for the San Bernardino epicenter. For the San Bernardino traces, we see on the eastern components of motion, a displacement of roughly 45 cm in 20 sec. Static offsets of 55 and 42 cm are observed for the smooth model on the east-west and north-south components, respectively. The random faults reach slightly different values owing to the distribution of the random displacements on the fault, i.e., the southern two-thirds of the fault largely control the static displacements. The sharp change in the direction of motion on the north-south component of the San Bernardino synthetics is a result of change in sign of the source radiation felt by the receivers as the double-couple propagates northward.

As the De Hoop-Haskell method calculates only the direct body waves, the synthetics do not include the considerable influence of moho refractions and reflections and crustal reverberations. These other body-wave arrivals are ignored in this present study to better enable an understanding of the effects of source complexity. The body-wave results presented may be viewed as lower bound estimates of the ground motion from the body waves.

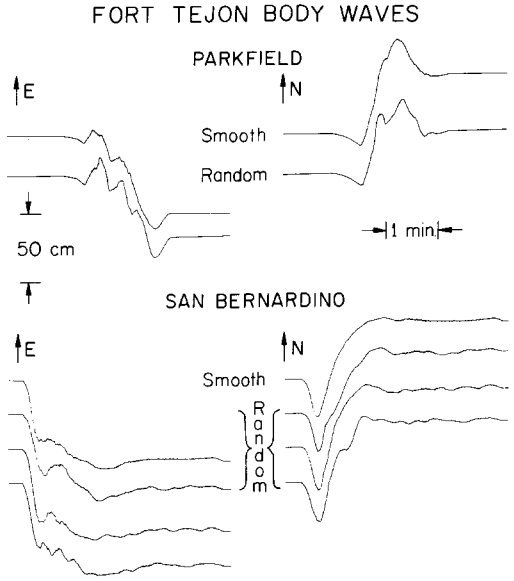

FIG. 3. Body-wave displacements (direct ray only) for a receiver in downtown Los Angeles.

SURFACE WAVES

The excitation of surface waves in a layered medium from a simple dislocation source has been completely formulated. One can use either the propagator matrices method developed by Harkrider (1964) and Ben-Menahem and Harkrider (1964) or by the asymptotic expressions for free oscillations used by Kanamori and Stewart (1976). The latter course is followed in this paper. This technique is briefly outlined below; for more details, the reader may refer to Appendix 1 of Kanamori and Stewart (1976).

The transverse component for Love waves excited by a point double-couple with a step-time function can be given by

$$U_\phi(\Delta, t) = \frac{1}{2\pi} \int_{-\infty}^{+\infty} C_L(\sigma) \exp(i\sigma t)\, d\sigma \tag{8a}$$

$$C_L(\sigma) = \frac{1}{\sqrt{\sin \Delta}} \exp\left(-\frac{\pi}{4} i\right) \exp\left(-i \frac{\sigma a \Delta}{c}\right) [p_L P_L^{(1)} + i q_L Q_L^{(1)}], \sigma \geqq 0 \quad (8b)$$

$$C_L(\sigma) = C_L^*(-\sigma), \sigma < 0 \quad (8c)$$

where Δ is the distance in radians, t is the time, σ is the angular frequency, a is the earth's radius, and c is the phase velocity. In the above, p_L and q_L are constants determined by the fault geometry and the azimuth of the receiver, and $P_L^{(1)}$ and $Q_L^{(1)}$ are the excitation functions which can be computed by normal mode theory given an earth model and source depth. Similarly, the vertical component of Rayleigh waves can be given by

$$U_r(\Delta, t) = \frac{1}{2\pi} \int_{-\infty}^{\infty} C_R(\sigma) \exp(i\sigma t)\, d\sigma \quad (9a)$$

$$C_R(\sigma) = \frac{1}{\sqrt{\sin \Delta}} \exp\left(\frac{\pi}{4} i\right) \exp\left(-\frac{\sigma a \Delta}{c}\right) [s_R S_R^{(1)} + p_R P_R^{(1)} + i q_R Q_R^{(1)}], \quad \sigma \geqq 0 \quad (9b)$$

$$C_R(\sigma) = C_R^*(-\sigma), \quad (9c)$$

where the $s_R, p_R, q_R, S_R^{(1)}, P_R^{(1)}$, and $Q_R^{(1)}$ are analogous to the $p_L, q_L, P_L^{(1)}$, and $Q_L^{(1)}$ defined for the Love waves. The radial component of the Rayleigh waves is much smaller than the Love waves for a vertical strike-slip source and is not included in the computation of horizontal surface waves.

In the modeling of the surface wave, earth model KHC2 (see Table 1) was used. The excitation functions $P_R^{(1)}$, $Q_R^{(1)}$, $S_R^{(1)}$, $P_L^{(1)}$, and $Q_L^{(1)}$ were calculated over a range of normal modes for periods for 1 to 500 sec for five discrete depths: 2, 5, 8, 12, and 15 km. A study was made of the relative excitation of overtone modes to the fundamental for the Rayleigh waves. For periods greater than about 15 sec, the overtones may be neglected. For periods less than 15 sec, the overtones have a contribution comparable to the fundamental mode. However, difficulties in mapping the overtone branches of the spheroidal modes for the KHC2 structure precluded their use in the synthetics. Swanger and Boore (1978) have studied the overtone contributions for Love waves. Their results indicate that the relative importance of the overtones is sensitive to structure, source depth, and distance between source and receiver. For the surface wave calculations in this study, only the fundamental modes are used. The excitation functions for the different depths were averaged to yield an effective vertical line source. Equations (8a) and (9a) were interpolated between the smoothly varying excitation functions to obtain the response at appropriate periods and then transformed to the time domain by Fast Fourier transform. As for the body waves, the fault geometry in Figure 2 was assumed. The fault was subdivided into 150 sections of 2.5 km each. The p_R, q_R, s_R, p_L, and q_L were then calculated for each segment using downtown Los Angeles as the receiver site. Attenuation was incorporated in the calculation by multiplying the integrals of equations (8a) and (9a) by

$$\exp\left(-\frac{\sigma d}{2QU}\right) \quad (10)$$

where d is the distance in kilometers to Los Angeles, U, the group velocity, and Q, the quality factor. A constant Q of 300 was used in this study. The source finiteness of each segment is accounted for by the inclusion in the integrals (8a) and (9a) of the factor

$$\frac{\sin(\sigma t_c/2)}{\sigma t_c/2} \tag{11}$$

where t_c is the rupture-time constant given by

$$t_c = \frac{L_s}{c}\left(\frac{c}{V_R} - \cos\theta\right) \tag{12}$$

with L_s, the fault segment length, c, the phase velocity, V_R, the rupture velocity, and θ, the azimuth of receiver measured from the rupture direction. By appropriately time-shifting and summing the effects of each segment for a chosen epicenter, a propagating rupture is produced.

The dislocation time function was assumed to be a linear ramp function of rise time τ, where $\tau = D/\dot{D}$. The excitation functions are calculated for a step time function. The correction for a finite rise time may be made with a further factor in equations (8a) and (9a) of

$$\frac{\sin\left(\frac{\sigma\tau}{2}\right)}{\frac{\sigma\tau}{2}}. \tag{13}$$

Synthetic Rayleigh waves are shown in Figure 4 for the Fort Tejon models listed in Table 2. Epicenters are chosen at Parkfield, Palmdale, and San Bernardino. Similarly, Figures 5 and 6 show, respectively, the north-south and east-west components of the Love waves. Two components are necessary to describe the Love waves as there is no true transverse component of motion due to the changing geometry between the source and receiver as the earthquake propagates. As with the body waves, we consider at this time a qualitative review of the surface wave synthetics and defer a more quantitative discussion to the next section.

Neither the Rayleigh nor the Love waves exhibit the customary well-dispersed waveforms observed at teleseismic distances for other earthquakes. The surface wave radiation pattern for both Rayleigh and Love waves for a vertical strike-slip double-couple is four-lobed. Thus, as the source propagates along the fault, the radiation felt by the receiver varies rapidly between loops and nodes. Therefore, even for the so-called smooth model, the synthetics have a complicated waveform.

Comparing the gross features of the Rayleigh and Love waves, while it is seen that the very long-period components ($T > 10$ sec) of both types are of the roughly comparable order of 10 cm, the Love waves exhibit an order of magnitude more energy in the seismic bands in which we are concerned, periods between 1 and 10 sec. At very long periods, a gross Love-to-Rayleigh wave amplitude ratio of 2 may be expected for a vertical pure strike-slip fault. For shallow faults, however, another factor plays a more important role for the period range of interest. By looking at the shape of the Rayleigh wave excitation functions appropriate for our Fort Tejon model, it is found that there is a sign change, or rather a node, between the free

surface and 15-km depth for periods between 1 and 10 sec. The Love wave excitation function has no node in this depth range. Consequently, the Love-to-Rayleigh ratio for this depth range is significantly amplified. This effect for the vertical pure strike-slip fault has previously been documented by Harkrider (1970), who noted that the nodal period in seconds of the Rayleigh to Love spectral ratio is roughly equal to the source depth in kilometers for this type of earthquake.

The Rayleigh wave synthetics for the smooth and random models are quite similar. This result is not unexpected in view of the above discussion. The very long-period components which make up the Rayleigh waves simply average over the heterogeneities in our model. The Love wave synthetics for the random models

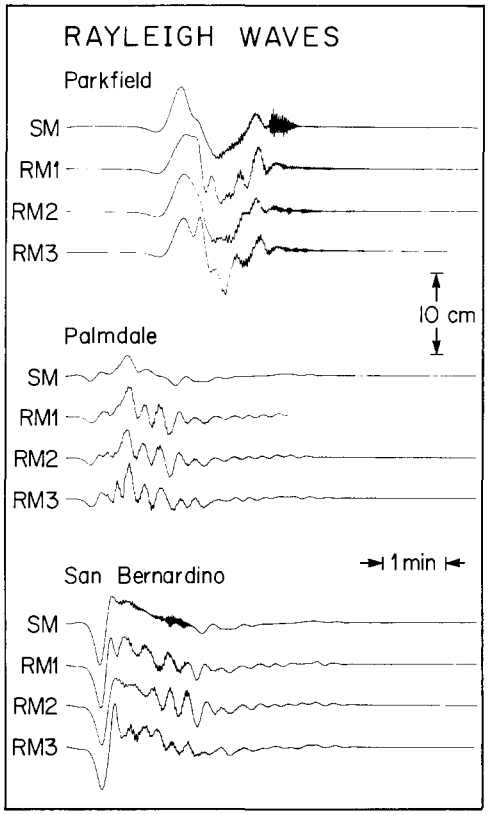

FIG. 4. Synthetic Rayleigh waves calculated for a receiver in downtown Los Angeles for the Fort Tejon models listed in Table 2. Epicenters are chosen at Parkfield, Palmdale, and San Bernardino (SM, smooth model; RM, random model.)

show considerably more structure than their corresponding smooth model. The energy between the periods 1 and 10 sec have wavelengths which are much more sensitive to the heterogeneities. The effect is not so much a boost of the maximum amplitude but is rather an increase in the duration of large amplitude motion.

Time and considerations of computing costs limited the number of long-period ground motion simulations for each random model. Nevertheless, while each simulation does not represent an average of all possible outcomes from an ensemble of random models, each synthetic represents a credible simulation of long-period ground motion for the assumptions stated above. Comparing the synthetics for the three random models, it is noted that the visual characteristics are quite similar. In the following section, amplitudes and durations obtained from band-pass filtering

the synthetics do not yield systematic or significant differences among the random models. This result suggests that although the addition of randomness is quite important in the determination of amplitudes and durations of ground motion, the synthetics are not particularly sensitive to the specific parameters of the random variation along the fault.

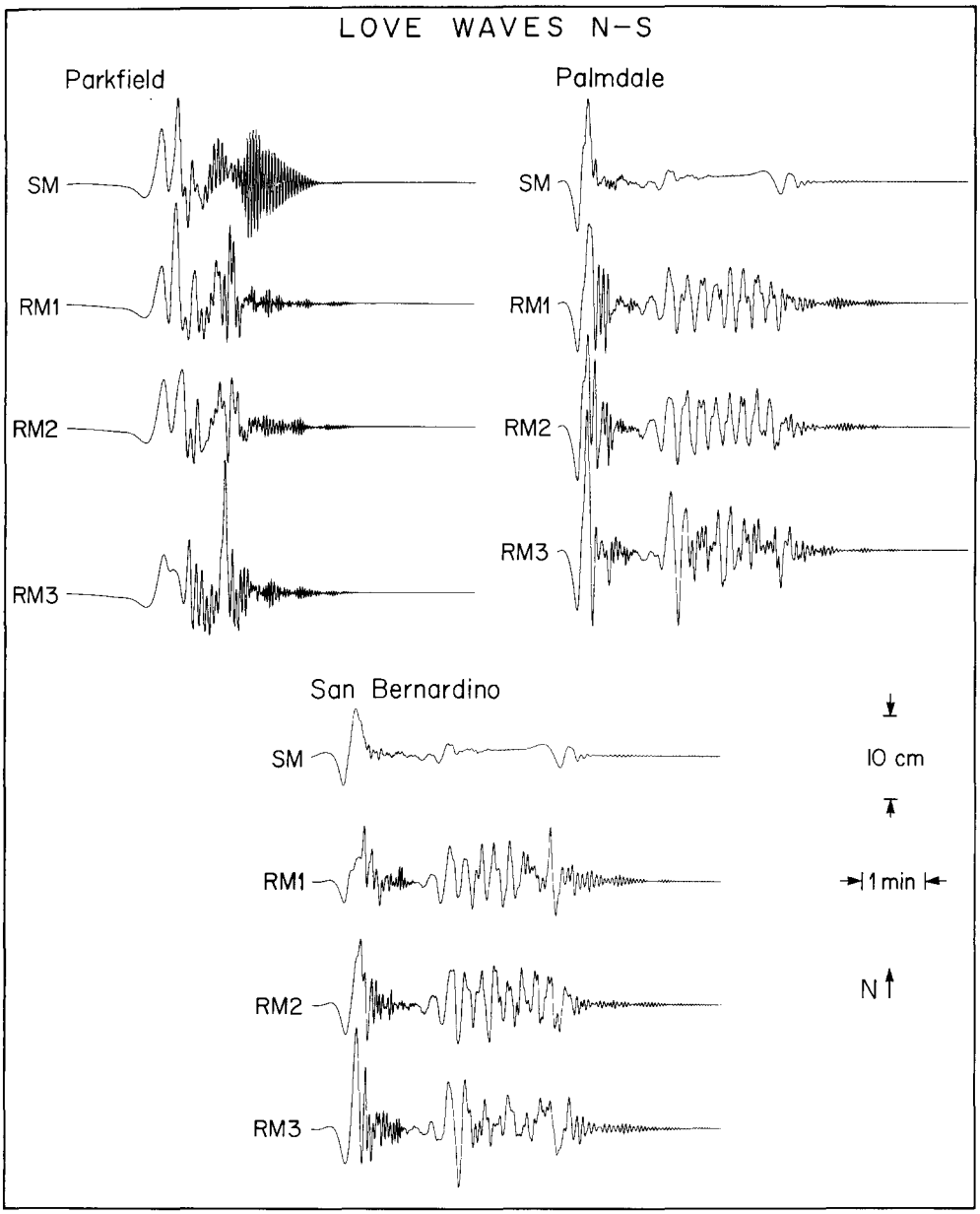

FIG. 5. Synthetic Love waves, north-south component, calculated for a receiver in downtown Los Angeles for the Fort Tejon models listed in Table 2.

In terms of the amplitude of ground motions from the surface waves, the location of the epicenter in the Fort Tejon models is not crucial. However, the location of the epicenter is important for estimating durations of ground motion. An epicenter at Parkfield probably represents the lower bound on duration, as the source moves

closer to Los Angeles as it ruptures. The synthetics for the Palmdale and San Bernardino epicenters, which are quite similar, represent the reverse situation and may be considered rough upper bounds on the duration of surface wave ground motion.

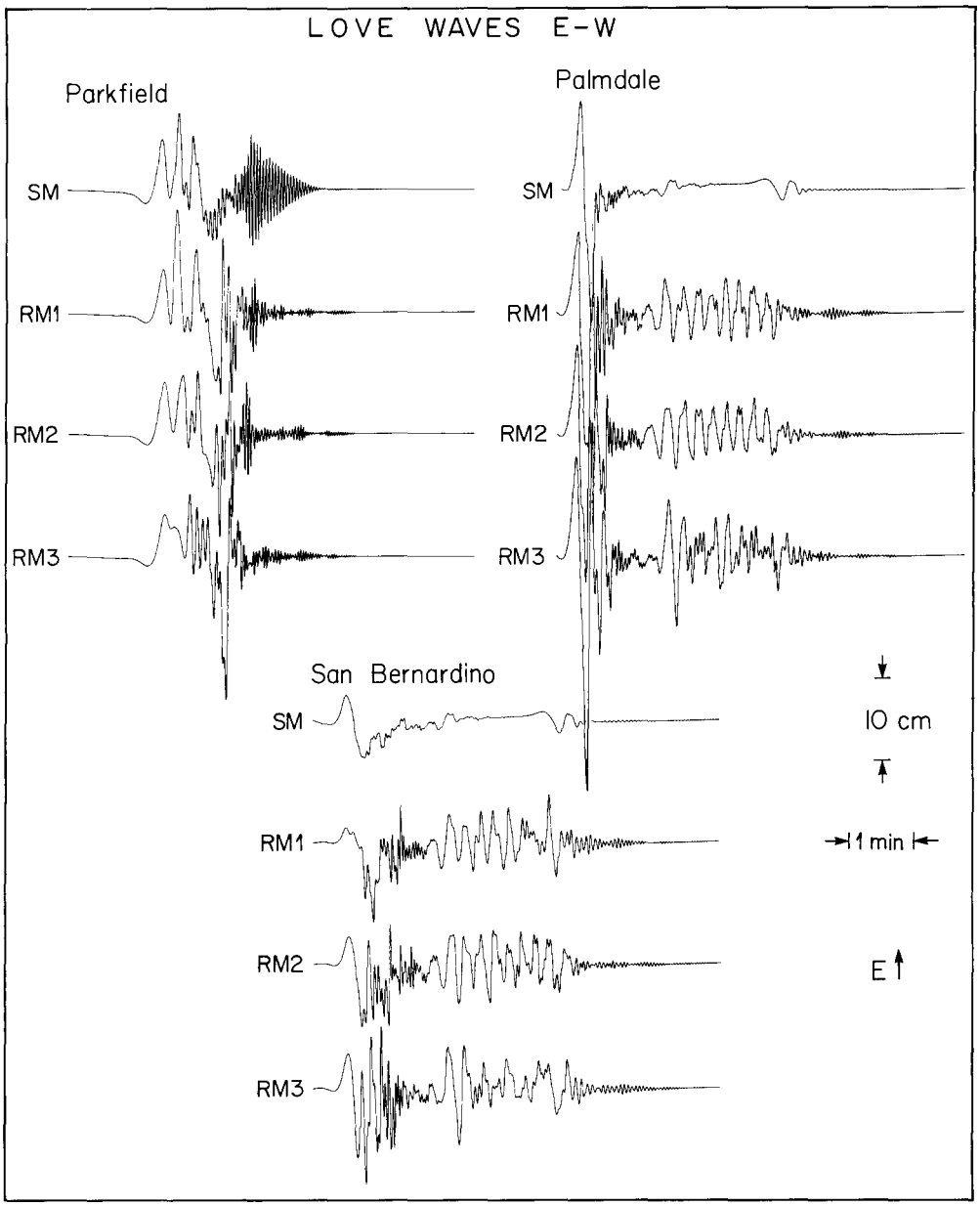

FIG. 6. Synthetic Love waves, east-west component, calculated for a receiver in downtown Los Angeles for the Fort Tejon models listed in Table 2.

DISCUSSION

To place the results of the Fort Tejon synthetics in some perspective, they are compared to a design earthquake. Traces (a) and (b) in Figure 7 show a Fort Tejon surface wave synthetic and design earthquake A-1 (Jennings *et al.*, 1968). Earthquake A-1 was generated by a random process with a prescribed acceleration power

spectral density, multiplied by envelope functions chosen to model the changing intensity of accelerations at the beginning and end of real accelerograms. The accelerations associated with earthquake A-1 were scaled such that the average value of the spectral intensity is 150 per cent as strong as the average spectrum intensity recorded on two accelerograms of the magnitude 7 El Centro earthquake of 1940. Earthquake A-1 "is designed to represent an upper bound for the ground motions expected in the vicinity of a causative fault during an earthquake having a Richter magnitude of 8 or greater". In comparison, the amplitude of ground motion of the design earthquake is roughly twice that of the Fort Tejon synthetics. However, the duration of ground motion for the Fort Tejon synthetics is considerably longer than the upper bound of 120 sec set for the design earthquake. The shorter duration

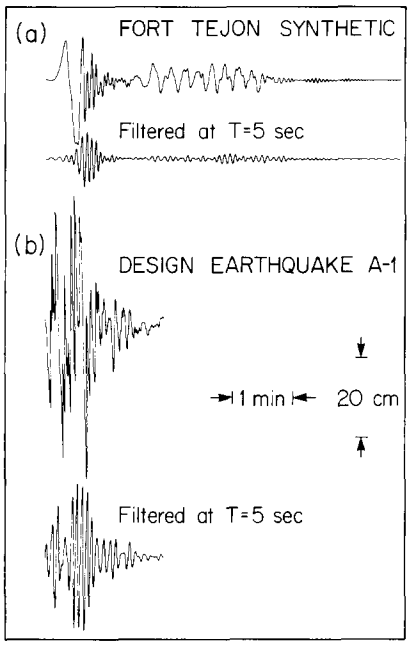

FIG. 7. Comparison of a Fort Tejon synthetic with design earthquake A-1 (Jennings *et al.*, 1968). The filtered traces were obtained using a Gaussian filter peaked at 5 sec.

of the design earthquake is due to using acceleration criteria in estimating duration. At a period of 5 sec, displacement amplitudes of 1 cm yield accelerations of 0.2 per cent g, a value quite small relative to high-frequency accelerations. Although the long period accelerations are low, the effects are significant over long durations. Displacement or velocity criteria yield more meaningful estimates of long-period ground motion durations.

To quantify the results, the Fort Tejon body and surface wave synthetics were narrow band-pass filtered using a Gaussian filter. Three periods of interest were chosen for the filtering; 3, 5, and 7 sec. Figure 7 illustrates the effect of the 5-sec filter on a synthetic and the design earthquake. We may characterize each of the filtered synthetics by two gross measures; the maximum peak-to-peak amplitude and the "scaled duration" of the ground motion. The scaled duration is defined as the length of time for which the amplitude of the ground motion is greater than 10 per cent of the maximum amplitude.

Figures 8 to 10 plot the maximum amplitude versus the scaled duration for the

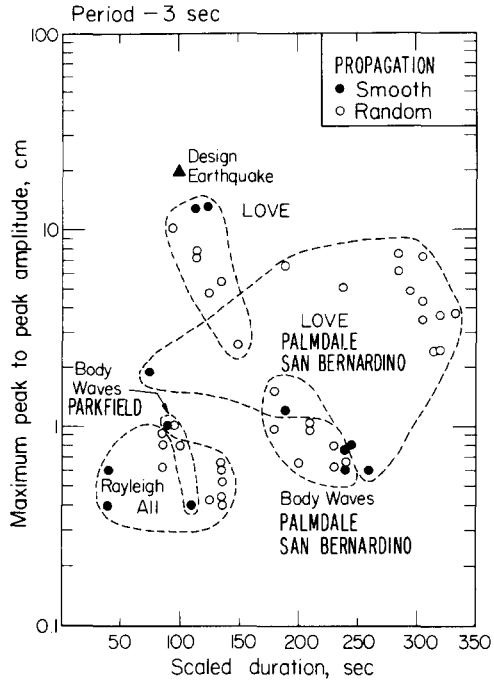

FIG. 8. Maximum amplitude versus scaled duration for the synthetics in Figures 4 to 6 filtered at 3 sec. Smooth and random propagation models are designated. The dashed lines qualitatively group the data.

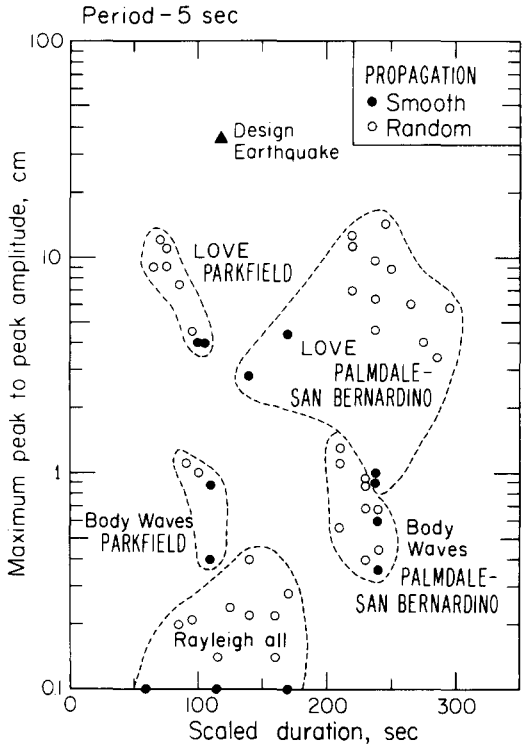

FIG. 9. Maximum amplitude versus scaled duration for the synthetics in Figures 4 to 6 filtered at 5 sec. Smooth and random propagation models are designated. The dashed lines qualitatively group the data.

synthetics and the design earthquake for filters at 3-, 5-, and 7-sec periods, respectively. The points are grouped only to indicate wave type and epicenter, and *not* to imply a range limitation. There were no systematic differences between the Palmdale and San Bernardino epicenters for the Love waves and for the body waves, among the three epicenters for the Rayleigh waves, between the north-south and east-west components of the Love waves, or among the three different random models. Therefore, no distinct categories are made from these groups.

First consider the ground motion at a period of 5 sec (Figure 9). The Love wave radiation is by far the most important seismic energy radiated at 5 sec, being an order of magnitude larger in amplitude than either the body waves or Rayleigh waves. The maximum amplitudes for the Love waves are similar for epicenters at

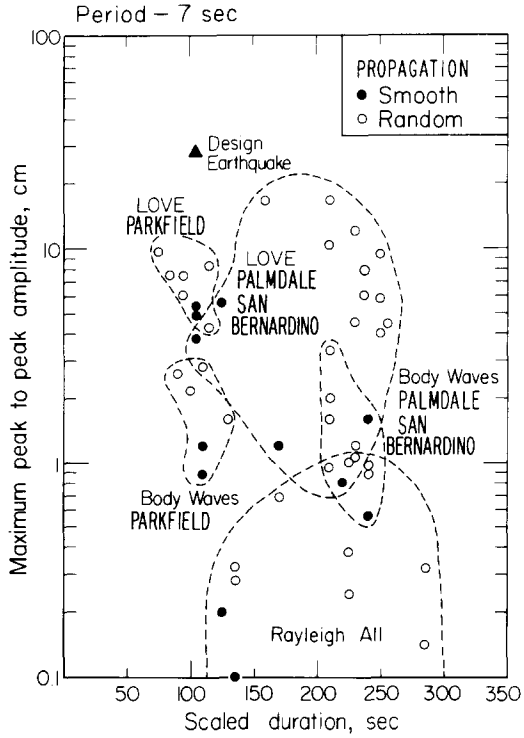

FIG. 10. Maximum amplitude versus scaled duration for the synthetics in Figures 4 to 6 filtered at 7 sec. Smooth and random propagation models are designated. The dashed lines qualitatively group the data.

either end of the fault, roughly 4 to 15 cm for most synthetics. The random models have considerably larger amplitudes associated with them. The location of the epicenter plays an important role in the scaled duration of ground motion. An epicenter at Parkfield has a scaled duration of some 80 sec, while Palmdale or San Bernardino epicenters may have scaled durations of up to 300 sec. The design earthquake A-1 is plotted as the triangle in the *upper* part of the figure. Although the amplitudes of earthquake A-1 are large, the scaled duration may be more than a factor of 3 shorter than the Love wave synthetics.

The results for filtered periods at 3 and 7 sec (Figures 8 and 10) are similar to those found at 5 sec. Love waves still play the most important role both in terms of maximum amplitude and scaled duration. The design earthquake significantly

underestimates scaled durations at both 3- and 7-sec filtered periods. For 3-sec Love waves, scaled durations of up to 5½ min are credible.

Before summarizing the results, it is important to attempt to qualitatively estimate what effects possible misassumptions and obvious shortcomings have on this study. The body-wave calculations in this paper included only direct P and S waves and ignored crustal and moho refractions and reflections. Only the fundamental mode was used in the surface wave calculations. Thus, the amount of radiated seismic energy was underestimated. A laterally homogeneous structure was assumed in the calculations. Crustal heterogeneities could act as scatterers and diminish maximum amplitudes, although the scaled durations would probably increase. A low-velocity zone in the southern Californian crust would tend to trap energy near the surface and increase surface wave amplitudes, although this would be period-dependent. The local effect of the Los Angeles Basin is unknown. Finally, randomness was added to our models in an *ad hoc* manner. Although the synthetics were not sensitive to the parameters chosen for the random models, we cannot rule out finding somewhat different results if randomness was added in a different manner.

Finally, some prepublication results of Kanamori (1979) lend support to the results presented here. In this study, Kanamori models a Fort Tejon-size earthquake on the San Andreas Fault by dividing the fault into a number of discrete, smaller subevents. The ground motion for these smaller subevents is empirically modeled using displacement records from intermediate-size California earthquakes. The rupture process of a large Fort Tejon-size event is simulated by time lagging and adding the scaled ground motions for these discrete subevents. The ground motions obtained by this more empirical method are somewhat larger than obtained in the study presented here, but the overall agreement is quite satisfactory.

Summary

Tentative results have been presented toward an understanding of long-period ground motion in Los Angeles from a great earthquake on the San Andreas Fault. In the period band, 3- to 7-sec, ground motion from Love radiation is found to be most important, with peak-to-peak amplitudes up to 14 cm and scaled durations up to 5 min. Although the amplitudes obtained for the ground motion are smaller than previous design earthquakes, the durations are longer by 2+ min. The inclusion of some complexity in the earthquake source is found to significantly enhance the amplitudes and durations of the long-period ground motion for the models assumed. The amplitudes are not particularly sensitive to the epicenter, whereas durations for a San Bernardino epicenter are significantly longer than Parkfield epicenters. As only the direct body waves and fundamental surface waves were used in the analysis, the amplitudes of the ground motion should be considered lower bounds for the models presented. Uncertainties in details of the rupture process and the local crustal structure preclude more definitive conclusions at this time.

Acknowledgments

Rhett Butler was supported by a Fannie and John Hertz Foundation Fellowship and the U.S. Department of Agriculture. The research was supported by U.S. Geological Survey Contracts 14-08-0001-16776, 14-08-0001-17631, and 14-08-001-18321, Division of Geological and Planetary Sciences, California Institute of Technology, Pasadena, California 91125.

References

Abe, K. (1974). Seismic displacement and ground motion near a fault: the Saitama earthquake of September 21, 1931, *J. Geophys. Res.* **79,** 4393–4399.

Agnew, D. C. and K. E. Sieh (1978). A documentary study of the felt effects of the great California earthquake of 1857, *Bull. Seism. Soc. Am.* **68,** 1717.

Aki, K. (1967). Scaling law of seismic spectrum, *J. Geophys. Res.* **72,** 1217–1231.

Aki, K. (1968). Seismic displacements near a fault, *J. Geophys. Res.* **73,** 5359–5376.

Anderson, D. L. and R. S. Hart (1976). An earth model based on free oscillations and body waves, *J. Geophys. Res.* **81,** 1461–1475.

Ben-Menahem, A. and D. G. Harkrider (1964). Radiation patterns of seismic surface waves from buried dipolar point sources in a flat stratified earth, *J. Geophys. Res.* **69,** 2605–2620.

Burdick, L. J. and G. R. Mellman (1976). Inversion of the body waves from the Borrego Mountain earthquake to the source mechanism, *Bull. Seism. Soc. Am.* **66,** 1485–1499.

Butler, R., G. S. Stewart, and H. Kanamori (1979). The July 27, 1976 Tangshan, China earthquake—A complex sequence of intraplate events, *Bull. Seism. Soc. Am.* **69,** 207–220.

De Hoop, A. T. (1958) Representation theorems for the displacement in an elastic solid and their application to elastodynamic diffraction theory, *Ph.D. Thesis,* Technische Hogeschool, Delft.

Ebel, J. E., L. J. Burdick, and G. S. Stewart (1978). The source mechanism of the August 7, 1966 El Golfo earthquake, *Bull. Seism. Soc. Am.* **68,** 1281–1292.

Geller, R. J. (1976). Scaling relations for earthquake source parameters and magnitudes, *Bull. Seism. Soc. Am.* **66,** 1501–1523.

Hanks, T. C. (1976). Observations and estimation of long-period strong ground motion in the Los Angeles basin, *Earthquake Eng. Struct. Dyn.* **4,** 473–488.

Harkrider, D. G. (1964). Surface waves in multilayered elastic media. I. Rayleigh and Love waves from buried sources in a multilayered elastic half-space, *Bull. Seism. Soc. Am.* **54,** 627.

Harkrider, D. G. (1970). Surface waves in a multilayered elastic media. Part II. Higher mode spectra and spectral ratios from point sources in plane layered earth models, *Bull. Seism. Soc. Am.* **60,** 1937.

Haskell, N. (1964). Total energy and energy spectral density of elastic wave radiation from propagating faults, *Bull. Seism. Soc. Am.* **54,** 1811–1841.

Haskell, N. (1966). Total energy and energy spectral density of elastic wave radiation from propagating faults, *Bull. Seism. Soc. Am.* **56,** 125–140.

Haskell, N. (1969). Elastic displacements in the near-field of a propagating fault, *Bull. Seism. Soc. Am.* **59,** 865–908.

Heaton, T. H. and D. V. Helmberger (1977). A study of the strong ground motion of the Borrego Mountain, California earthquake, *Bull. Seism. Soc. Am.* **67,** 315–330.

Heaton, T. H. and D. V. Helmberger (1978). Predictability of strong ground motion in the Imperial Valley; modeling the *M*4.9, November 4, 1976 Brawley earthquake, *Bull. Seism. Soc. Am.* **68,** 31–48.

Helmberger, D. V. and S. D. Malone (1975). Modeling local earthquakes as shear dislocations in a layered half-space, *J. Geophys. Res.* **80,** 4881–4888.

Herrmann, R. B. and O. W. Nuttli (1975a). Ground-motion modeling at regional distances for earthquakes in a continental interior, I. Theory and observations, *Earthquake Eng. Struct. Dyn.* **4,** 49–58.

Herrmann, R. B. and O. W. Nuttli (1975b). Ground-motion modeling at regional distances for earthquakes in a continental interior, II. Effect of focal depth, azimuth and attenuation, *Earthquake Eng. Struct. Dyn.* **4,** 59–72.

Jennings, P. C., G. W. Housner, and N. C. Tsai (1968). Simulated earthquake motions, National Science Foundation report, *Earthquake Eng. Res. Lab.,* California Institute of Technology, Pasadena.

Kanamori, H. (1970). Synthesis of long-period surface waves and its application to earthquake source studies, Kurile Islands earthquake of October 13, 1963, *J. Geophys. Res.* **75,** 5011–5027.

Kanamori, H. (1972). Determination of effective tectonic stress associated with earthquake faulting: the Tottori earthquake of 1943, *Phys. Earth Planet. Interiors* **5,** 426–434.

Kanamori, H. (1977). The energy release in great earthquakes, *J. Geophys. Res.* **82,** 2981–2987.

Kanamori, H. (1979). Semi-empirical approach to prediction of long-period ground motion, *Bull. Seism. Soc. Am.* **69,** 1645–1670.

Kanamori, H. and J. J. Cipar (1974). Focal process of the Great Chilean earthquake May 22, 1960, *Phys. Earth Planet. Interiors* **9,** 128–136.

Kanamori, H. and D. Hadley (1975). Crustal structure and temporal velocity change in southern California, *Pageoph* **113,** 257–280.

Kanamori, H. and G. S. Stewart (1976). Mode of the strain release along the Gibbs fracture zone, Mid-Atlantic Ridge, *Phys. Earth Planet. Interiors* **11,** 312–332.

Kanamori, H. and G. S. Stewart (1978). Seismological aspects of the Guatemala earthquake of February 4, 1976, *J. Geophys. Res.* **83,** 3427–3434.

Langston, C. A. (1977). A body wave inversion of the Koyna, India earthquake of December 10, 1967 and some implications for body wave focal mechanisms, *J. Geophys. Res.* **81,** 2517–2529.

Langston, C. A. (1978). The February 9, 1971 San Fernando earthquake, a study of source finiteness in teleseismic body waves, *Bull. Seism. Soc. Am.* **68,** 1.

Langston, C. A. and R. Butler (1977). Focal mechanism of the August 1, 1975 Oroville earthquake, *Bull. Seism. Soc. Am.* **66,** 111.

Mikumo, T. (1973a). Faulting mechanism of the Cifu earthquake of September 9, 1969 and some related problems, *J. Phys. Earth.* **21,** 191–212.

Mikumo, T. (1973b). Faulting process of the San Fernando earthquake of February 9, 1971 inferred from static and dynamic near-field displacements, *Bull. Seism. Soc. Am.* **63,** 249–269.

Rial, J. A. (1978). The Caracas, Venezuela earthquake of July 1967: a multiple source event, *J. Geophys. Res.* **83,** 5405.

Sieh, K. (1978). Slip along the San Andreas fault associated with the great 1857 earthquake, *Bull. Seism. Soc. Am.* **68,** 1421.

Stewart, G. S. (1978). Implications for plate-tectonics of the August 19, 1977 Indonesian decoupling normal-fault earthquake (abstract), *EOS, Trans. Am. Geophys. Union* **59,** 326.

Stewart, G. S. and S. N. Cohn (1978). The August 16, 1976 Mindanao, Philippine earthquake (M_S = 7.8)—Evidence for a subduction zone south of Mindanao, *Geophys. J.* **57,** 51.

Swanger, H. J. and D. M. Boore (1978). Simulation of strong-motion displacements using surface wave modal superposition, *Bull. Seism. Soc. Am.* **68,** 907–922.

Trifunac, M. D. (1974). A three-dimensional dislocation model for the San Fernando, California earthquake of February 9, 1971, *Bull. Seism. Soc. Am.* **64,** 149–172.

Wallace, R. E. (1968). Notes on stream channels offset by the San Andreas fault, southern coast ranges, California, in *Proceedings of Conference on Geologic Problems of the San Andreas Fault System*, W. R. Dickinson and A. Grantz, Editors, Stanford Univ. Publ., *Geol. Sci., Univ. Ser.* **11,** 6–21.

Wood, H. O. (1955). The 1857 earthquake in California, *Bull. Seism. Soc. Am.* **45,** 47–67.

SEISMOLOGICAL LABORATORY
CALIFORNIA INSTITUTE OF TECHNOLOGY
PASADENA, CALIFORNIA 91125
CONTRIBUTION NO. 2920

Manuscript received January 29, 1979